Chemical Science

ROYAL SOCIETY OF CHEMISTRY

EDGE ARTICLE

View Article Online
View Journal | View Issue

Cite this: *Chem. Sci.*, 2024, **15**, 15255

All publication charges for this article have been paid for by the Royal Society of Chemistry

Received 17th May 2024
Accepted 19th August 2024

DOI: 10.1039/d4sc03235g

rsc.li/chemical-science

Absolute control over the quantum yield of a photodissociation reaction mediated by nonadiabatic couplings

Ignacio R. Sola *[a] and Alberto García-Vela *[b]

Control of molecular reaction dynamics with laser pulses has been developed in the last decades. Among the different magnitudes whose control has been actively pursued, the branching ratio between different product channels constitutes the clearest signature of quantum control. In polyatomic molecules, the dynamics in the excited state is quagmired by non-adiabatic couplings, which are not directly affected by the laser, making control over the branching ratio a very demanding challenge. Here we present a control scheme for the CH_3I photodissociation in the A band, that modifies the quantum yield of the two fragmentation channels of the process. The scheme relies on the optimized preparation of an initial superposition of vibrational states in the ground potential, which further interfere upon the excitation with a broad pump pulse. This interference can suppress any of the channels, regardless of its dominance, and can be achieved over the whole spectral range of the A band. Furthermore, it can be accomplished without strong fields or direct intervention during the dynamics in the excited states: the whole control is predetermined from the outset. The present work thus opens the possibility of extensive and universal control of the channel branching ratio in complex photodissociation processes.

Introduction

Quantum control of molecular reaction dynamics has been actively pursued over the last decades.[1–11] Among these reactions, the near ultraviolet photolysis of CH_3I in the first absorption band (the A band, ranging from 220 to 350 nm with a maximum at about 260 nm) has been considered as a prototypical photodissociation reaction. The relatively small size of this polyatomic molecule favors its study both experimentally and theoretically. In addition, the presence of a conical intersection between the two main excited valence states produces interesting nonadiabatic effects in the photodissociation dynamics. The A band absorption spectrum of CH_3I was measured almost fifty years ago.[12] After this pioneering work, a variety of experimental techniques were applied to investigate the CH_3I photodissociation dynamics in the A band. This process was the first one investigated by ion imaging by Chandler and Houston[13] at 266 nm, later followed by velocity map imaging (VMI) measurements by Eppink and Parker[14,15] over nearly the whole band (240–334 nm). Time-resolved studies were pioneered by Zewail and coworkers,[16] and then a series of time-resolved VMI experiments were reported for different regions of the A band.[17–20] Photoelectron imaging experiments in the range 245.5–261.6 nm were also reported.[21] The first theoretical study on the photolysis dynamics of CH_3I in the A band consisted of a two-dimensional wave packet model by Shapiro and Bersohn.[22] This model was later improved by Guo,[23] by adding a third degree of freedom. Then, wave packet models including four,[20] five,[24] and the full nine[25] dimensions of the system were reported. Those models used either the six-dimensional,[26] or the full-dimensional,[27] *ab initio* potential-energy surfaces of CH_3I calculated by Morokuma and coworkers, further refined by Xie *et al.*[28]

Quantum control of molecular processes takes advantage of the coherent properties of light. Several control schemes applying both strong and weak laser fields have been proposed for different molecular reactions.[29–46] Rather surprisingly, control of the prototypical photodissociation dynamics of CH_3I has been the subject of very few works. In fact, to the best of our knowledge only two theoretical[31,47] only one theoretical[31] and two experimental[43,45] quantum control works on the CH_3I photolysis in the A band have been reported. The two excited states mainly involved in the photodissociation, namely $^3Q_0$ and $^1Q_1$, are connected by a conical intersection and give rise to two different product channels forming $CH_3 + I^*(^2P_{1/2})$ and $CH_3 + I(^2P_{3/2})$, respectively. The branching ratio between these two channels should in principle be susceptible to be controlled. However, with the exception of ref. 31, 43 and 47, no attempts in this sense have been reported.

In this work we suggest a quantum control scheme that aims at modifying the branching ratio of the two product channels of

[a]*Departamento de Química Física, Universidad Complutense de Madrid (and Unidad Asociada I+D+I al CSIC), 28040 Madrid, Spain. E-mail: isolarei@ucm.es*

[b]*Instituto de Física Fundamental, Consejo Superior de Investigaciones Científicas, Serrano 123, 28006 Madrid, Spain. E-mail: garciavela@iff.csic.es*

the CH_3I photodissociation, $CH_3 + I^*(^2P_{1/2})$ and $CH_3 + I(^2P_{3/2})$, over the whole energy range of the A band. Recognizing the crucial role of the initial coherences in the control of ultrafast processes,[48–51] our scheme reverses the order of the pulses in the "orthodox" two-step approach. Instead of first applying a strong ultrashort pump pulse, which ignites the dynamics creating a vibronic wave packet in the excited states, and then the control pulse, guiding the dynamics by adjusting or modifying the phases along the reaction coordinate, as necessary (where in many practical implementations both pulses can be integrated into a single pulse of complex structure), we first apply a control pulse that prepares the coherences in the ground electronic state, and then use the ultrafast pump pulse to pump the proper wave packet in the desired excited state. The method can be seen as a generalization of one of the Brumer–Shapiro coherent control scenarios,[31] where we generate a superposition of vibrational states using the geometrical optimization (GO) procedure,[52–56] optimizing variationally the superposition coefficients in order to maximize a given functional which in our case is the desired branching ratio, either [I*]/([I*] + [I]) or [I]/([I*] + [I]), over the different wavelengths of the A band. This implies a different and more complex derivation of the optimal equations, leading to non-linear eigenvalue equations, as shown in the Methodology. The optimization procedure is driven by the output of wave packet simulations on the CH_3I photodissociation dynamics, and by the interference between the superposition coefficients. Since the control scheme applied relies on interference, only a weak laser field is required to pump CH_3I to the excited states, thus avoiding potential problems associated with intense fields. In this way, the control scheme suggested allows to maximize the yield of any of the two product channels at different wavelengths in the A band, with respect to the natural yield obtained in the absence of control.

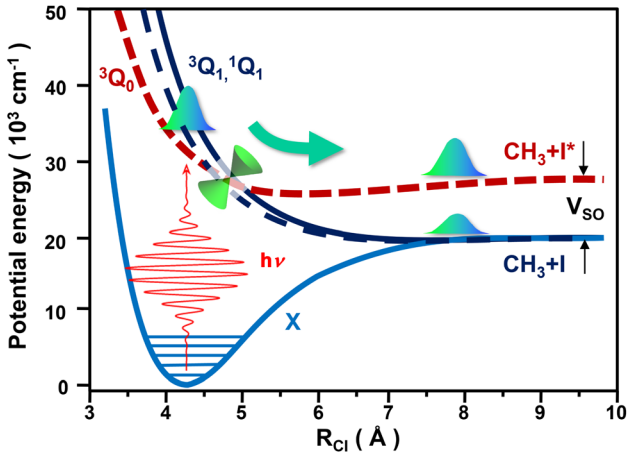

Fig. 1 Schematic picture of the CH_3I photodissociation process in the A band. The potential-energy curves along the C–I coordinate are shown for the four electronic states, $\tilde{X}^1A_1$, $^3Q_0$, $^1Q_1$, and $^3Q_1$, involved in the photodissociation of CH_3I in the A band. The location of the conical intersection between the $^3Q_0$ and $^1Q_1$ states is denoted by a double cone. The two asymptotes correlating with the CH_3 + I and CH_3 + I* fragments are separated by the iodine spin–orbit splitting, V_{SO}, indicated by the two black arrows. Laser excitation from the ground to the excited states is schematically represented. The CH_3I fragmentation dynamics is indicated graphically by the green arrow, including the bifurcation at the conical intersection of the wave packet initially pumped.

Methodology

The control scheme

Photodissociation of CH_3I in the A band involves a dominant parallel $^3Q_0 \leftarrow X^1A_1$ transition and two perpendicular transitions, $^1Q_1 \leftarrow X^1A_1$ and $^3Q_1 \leftarrow X^1A_1$, of lower intensity. The photodissociation process is schematically depicted in Fig. 1. The $^1Q_1$ and $^3Q_1$ states correlate asymptotically to the same fragments, $CH_3 + I(^2P_{3/2})$, while $^3Q_0$ correlates to the $CH_3 + I^*(^2P_{1/2})$ products. For simplicity, hereafter these two product channels will be referred to as the I and I* channels, respectively. The asymptote of $^3Q_0$ is separated from that of $^1Q_1$ and $^3Q_1$ by the iodine spin–orbit splitting, 0.943 eV.[14] In addition, a conical intersection (CI) connects the $^3Q_0$ and $^1Q_1$ states, so a wave packet initially excited to any of these two states will bifurcate at the CI, producing both CH_3 + I and CH_3 + I* fragments.

In the following, we describe briefly the GO procedure on which the control scheme applied in this work is based. The cross section for the photodissociation of CH_3I in the electronic channel e (I or I*) can be written, in its time-dependent formulation, as

$$\sigma_v^{e,n}(E) = \frac{C\omega k_v^{e,n}}{2\pi}\left|\int_0^\infty \left\langle \psi_n^e(E)\middle|\hat{U}(t,0)\middle|\psi_v^g\right\rangle e^{iEt}dt\right|^2 \quad (1)$$

where ψ_n^e is the scattering wave function for channel e and energy E, with all vibrational and rotational quantum numbers of the fragments given collectively by n, $\hat{U}(t,0)$ is the time evolution operator, which depends on the pump pulse, $\varepsilon(t)$, with frequency ω, and ψ_v^g is the initial wave function, here assumed to be in the v vibrational state of the CH_3–I stretching mode. $k_v^{e,n}$ gives the relative speed of the fragments, constrained by the conservation of the total energy of the system, and C is a constant factor. While eqn (1) provides a compact form of the photodissociation cross section, a more detailed expression is given below.

We can write the expression for the total cross section in channel e in a very succinct way, as

$$\sigma_v^e(E) \propto \sum_n k_v^{e,n}\left\langle \Phi_v(E)\middle|\hat{S}_{e,n}\middle|\Phi_v(E)\right\rangle, \quad (2)$$

where $\hat{S}_{e,n} = \left|\psi_n^e(E)\right\rangle\left\langle\psi_n^e(E)\right|$ is the projection operator over the desired scattering state, and

$$|\Phi_v(E)\rangle = \int_0^\infty \hat{U}(t,0)\left|\psi_v^g\right\rangle e^{iEt}dt \quad (3)$$

is the function containing all the dynamical information of the photodissociation process. Defining the complex magnitude $A_v^{e,n}(E) = \sqrt{k_v^{e,n}}\langle\psi_n^e(E)|\Phi_v(E)\rangle$, eqn (2) becomes $\sigma_v^e(E) \propto \sum_n A_v^{e,n*}A_v^{e,n}$. Now, if instead of a single eigenstate, the initial state is a coherent superposition of N vibrational

eigenstates of the ground state potential $\psi(0) = \sum_j^N c_j \psi_j^g$, the photodissociation cross section will be proportional to

$$\sigma^e(E) \propto \sum_n \sum_j \sum_k c_j^* c_k \left\langle \Phi_j(E) \middle| \hat{S}_{e,n} \middle| \Phi_k(E) \right\rangle = \sum_n \sum_j \sum_k c_j^* c_k A_j^{e,n*} A_k^{e,n} = \mathbf{c}^\top \mathbf{S}^e \mathbf{c} \quad (4)$$

where we defined the scattering matrix $\mathbf{S}^e$, with elements $S_{jk}^e = \sum_n \Phi \left| S_{e,n} \right| \Phi\rangle = \sum_n A_j^{e,n*} A_k^{e,n}$, and the coefficients of the superposition were arranged as a column vector $\mathbf{c}$ (or its conjugate transpose row vector $\mathbf{c}^\mathrm{T}$). As long as $\mathbf{S}^e$ has non-diagonal elements, σ^e will exhibit interference patterns, such that one can maximize the quantum yield over the desired channel by optimizing the initial superposition state.

To do so, we define a functional of the quantum yield on channel I, $\chi^\mathrm{I} = \sigma^\mathrm{I}/\sigma_\mathrm{dis}$, where the total photodissociation cross section is $\sigma_\mathrm{dis} = \sigma^\mathrm{I} + \sigma^{\mathrm{I}^*}$, and we calculate its gradient with respect to $\mathbf{c}^\mathrm{T}$ (or $\mathbf{c}$). Imposing constraints over the norm of the initial wave function, $\mathbf{c}^\mathrm{T}\mathbf{c} = 1$, we obtain the nonlinear eigenvalue equation

$$\frac{1}{\sigma_\mathrm{dis}} \left(\mathbf{S}^\mathrm{I} - \chi^\mathrm{I} \mathbf{S}^\mathrm{I} - \chi^\mathrm{I} \mathbf{S}^{\mathrm{I}^*} \right) \mathbf{c} = \lambda \mathbf{c} \quad (5)$$

The maximum yield can be obtained from the eigenvector with largest eigenvalue $\mathbf{c}_\mathrm{op}$, which provides the optimal initial superposition $\Psi(0)$, as

$$\chi_\mathrm{op}^\mathrm{I} = \frac{\mathbf{c}_\mathrm{op}^\top \mathbf{S}^\mathrm{I} \mathbf{c}_\mathrm{op}}{\mathbf{c}_\mathrm{op}^\top \mathbf{S}^\mathrm{I} \mathbf{c}_\mathrm{op} + \mathbf{c}_\mathrm{op}^\top \mathbf{S}^{\mathrm{I}^*} \mathbf{c}_\mathrm{op}} \quad (6)$$

Notice that $\Psi(0)$ is obtained in a completely different way from the optimal superpositions that maximize absolute yields, as found in previous derivations using the geometrical optimization.[52,53,56] The same procedure can be followed to maximize the quantum yield in channel I*.

Wave packet calculations

In the present dynamical simulations, methyl iodide is represented as a CXI pseudotriatomic molecule,[23] where the pseudoatom X = H_3 is located at the center-of-mass of the three H atoms. In this model, three degrees of freedom represented by the (R, r, θ) Jacobi coordinates are included, where the dissociation coordinate R is the distance between I and the CH_3 (or C–X) center-of-mass, r is the C–X distance and it represents the umbrella bend of the C–H_3 group (ν_2), and θ is the angle between the vectors associated with R and r and it represents the X–C–I bend (ν_6). The assumption of modeling the umbrella mode of the C–H_3 group in CH_3I as a C–X stretching has been justified by a number of theoretical works,[18–20,22,23,28] which were successful in reproducing most of the experimental data. In the simulations, zero total angular momentum ($J = 0$) is assumed for the system.

The Hamiltonian and the potential-energy surfaces (PES) have been described in detail elsewhere.[18,19] In summary, the $\bar{X}^1A_1$ ground state PES is represented as a sum of three potential interactions in the $R_{C–I}$ (the C–I internuclear distance), r, and θ coordinates, respectively. The interaction potential in the $R_{C–I}$ coordinate is taken from the two-dimensional (2D) ground-state potential for CH_3I, obtained by means of multireference spin–orbit configuration interaction *ab initio* calculations.[57] The potential interactions in the r, and θ coordinates are modeled by harmonic oscillator functions. For the $^3Q_0$ and $^1Q_1$ excited electronic states and the nonadiabatic coupling between them, we have used the *ab initio* surfaces reported by Xie *et al.*,[28] which are an improved version of the previous nine-dimensional surfaces of Amatatsu *et al.*,[27] where the remaining six coordinates are fixed at their equilibrium values. The 2D *ab initio* PES of Alekseyev *et al.*,[58] was used for the $^3Q_1$ excited state, modelling the θ dependence of the potential surface.[19] The electric-dipole moment functions coupling radiatively $\bar{X}^1A_1$ with the three excited electronic states were also taken from the work of Alekseyev *et al.*[58]

The dynamical simulations solve the time-dependent Schrödinger equation.[18,19] Computational details on the basis set used to represent the wave packet, on the calculation of the initial state, and on the wave packet propagation have been given elsewhere.[19] The initial states propagated consisted of the direct product $\varphi_v(R)$ $\rho(r, \theta)$, where $\rho(r, \theta)$ is the ground vibrational state associated with the r and θ coordinates, and $\varphi_v(R)$ is the vibrational state associated with the R mode. Six different initial vibrational states $\varphi_v(R)$ $\rho(r, \theta)$ with $v = 0$–5 were propagated. The initial state amplitude is pumped from X^1A_1 to the three excited states by means of a laser field of the form $\varepsilon(t) = A(t)\cos(\omega t + \phi)$, where $A(t)$ is a Gaussian function, ω is the photon frequency of the incident radiation, and $\phi = 0$ for simplicity. Three different excitation wavelengths were used, namely 316 nm (3.92 eV), 266 nm (4.66 eV), and 216 nm (5.74 eV). Four different laser pulses were applied with pulse durations of 5, 15, 30, and 60 fs (full width at half maximum, FWHM). The intensity of the pulses ranges in the weak-field regime (of the order of 10^9 W cm^{-2}). The intensity of the different pulses was scaled with appropriate factors to ensure a constant pulse area $\int \mathrm{d}t |\varepsilon(t)|^2$ in all the simulations. The wave packet propagation was carried out for a total time $t_\mathrm{f} = 300$ fs, with a time step of 0.1 fs. This propagation time ensures that all the wave packet amplitude reaches the asymptotic region.

Partial photodissociation cross sections are computed along time by projecting out the asymptotic wave packet onto the corresponding fragment states, by means of the method of Balint-Kurti *et al.*[59,60]

$$\sigma_v^{i,\nu,j}(E) = \frac{C\omega k_v^{i,\nu,j}}{2\pi} \left| \int_0^{t_\mathrm{f}} \left\langle \chi_\nu^{(j)}(r) P_j(\cos\theta) \middle| \Psi_{i,v}(R_\mathrm{c}, r, \theta, t') \right\rangle \mathrm{e}^{iEt'/\hbar} \mathrm{d}t' \right|^2, \quad (7)$$

where C is a constant factor, ω is the incident photon frequency (corresponding to $\lambda = 316$, 266 and 216 nm), $i = 1$–3 denotes the three excited electronic states, ν is the initial vibrational state in the CH_3–I stretch mode, R_c is a suitably large distance of the dissociation coordinate R, E is the total energy of the system

reached with each excitation wavelength, $E = E_i + \hbar\omega$ (being E_i the energy of the CH_3I initial state), and $k_v^{i,v,j}$ is given by

$$k_v^{i,v,j} = [2m(E - V_{SO}\delta_{i1} - E_{v,j})]^{1/2}, \quad (8)$$

with V_{SO} the spin–orbit splitting between the two lowest electronic states of iodine, and δ_{i1} the Kronecker delta. The eigenstates of the CH_3 fragment (the C–X pseudodiatomic molecule) are represented by the product $\chi_v^{(j)}(r)P_j(\cos\theta)$, where $\chi_v^{(j)}(r)$ are the rovibrational states of C–X in the umbrella mode (with associated rovibrational energies $E_{v,j}$) and $P_j(\cos\theta)$ are Legendre polynomials. $\Psi_{i,v}(R_c, r, \theta, t')$ is the wave packet in the excited electronic state i at time t'. Eqn (7) is the expanded form of the more compact eqn (1). In the same way, the expanded form of $A_v^{e,n}(E)$ that appears in eqn (2) [or $A_j^{e,n}(E)$ and $A_k^{e,n}(E)$ that appear in eqn (4)] is

$$A_v^{i,v,j}(E) = \sqrt{\frac{C\omega k_v^{i,v,j}}{2\pi}} \int_0^{t_f} \left\langle \chi_v^{(j)}(r)P_j(\cos\theta) \middle| \Psi_{i,v}\left(R_c, r, \theta, t'\right) \right\rangle e^{iEt'/\hbar} dt'. \quad (9)$$

In order to calculate $A_v^{i,v,j}(E)$, the energy range E of the bandwidths associated with the four pulses of 5, 15, 30, and 60 fs applied are represented by a grid of 67 energy points, and the initial superposition is optimized for each of these energies of the grid.

Results and discussion

Photodissociation of CH_3I in the absence of control

The photodissociation dynamics of CH_3I in the A band has been computed for six different initial vibrational states of the ground electronic potential, corresponding to the v = 0–5 vibrations of the CH_3–I stretching mode. From these simulations, the corresponding $A_v^{e,n}(E)$ quantities are obtained (see the Methodology section), and with them, the optimized quantum yields of the I and I* channels are found by means of eqn (4)–(6). Before discussing the results of the optimization, it is interesting to analyze the absorption spectra calculated from a single vibrational state v, *i.e.*, in the absence of control, when the photodissociation cross section is obtained with eqn (1) instead of (4). Such spectra are displayed in Fig. 2 for the initial states corresponding to v = 0–5. Each panel of Fig. 2 shows three spectra corresponding to the $^3Q_0$, $^1Q_1$, and $^3Q_1$ electronic states. The spectra are calculated as the square of the Fourier transform of the autocorrelation function of the time-dependent wave packet evolving on each excited electronic state. We note that the $^3Q_0$ state contributes to the I* fragmentation channel, while both the $^1Q_1$ and $^3Q_1$ states contribute to the I channel.

The three spectra associated with each v state reflect the nodal pattern of the corresponding vibrational wave function, as expected from the reflection principle in repulsive electronic states.[61] The absorption spectrum of CH_3I was measured by Gedanken and Rowe,[12] and they found that the ratio between the maximum of intensity of the sub-bands associated with the $^3Q_0$, $^1Q_1$, and $^3Q_1$ states were 300 : 70 : 3, respectively. From the spectra of Fig. 2, it is seen that, when using the best currently available *ab initio* potential-energy surfaces, as done in the present work, the intensity of the $^1Q_1$ and $^3Q_1$ sub-bands is overestimated (and particularly that of $^3Q_1$). The population of the different v states is determined by a Boltzmann distribution at the temperature at which CH_3I is prepared in the photodissociation experiment. At typical experimental temperatures, most of the population of this distribution is at $v = 0$, and drops very fast for $v > 0$. Thus the CH_3I absorption spectrum in the A band is essentially dominated by that corresponding to $v = 0$. Indeed, this is why the spectra of the $v = 0$ panel of Fig. 2 are quite similar to those measured by Gedanken and Rowe[12] (leaving apart the differences in intensity of the $^1Q_1$ and $^3Q_1$ sub-bands; see Fig. 4 of ref. 12).

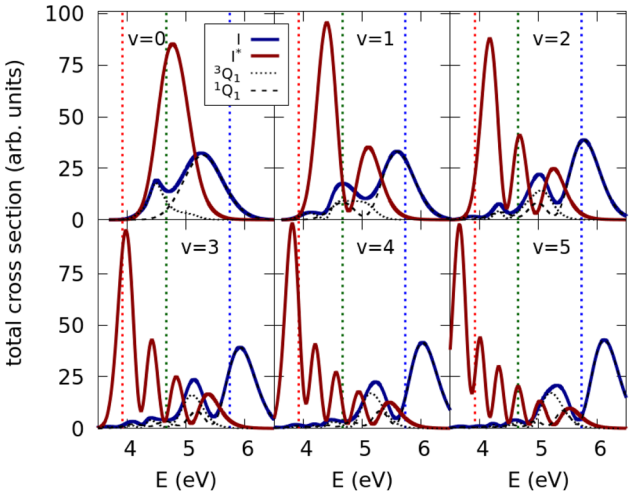

Fig. 2 Theoretical absorption spectra of CH_3I for the initial vibrational states $v = 0$–5 of the CH_3–I stretching mode. The absorption spectra calculated for the $^3Q_0$ (red thick solid line), $^1Q_1$ (black dashed line), and $^3Q_1$ (black short-dashed line) states are shown in the figure for the six first vibrational states $v = 0$–5 of the CH_3–I stretching mode. The sum of the $^1Q_1$ and $^3Q_1$ spectra, that corresponds to the I fragment channel, is also displayed (blue thick solid line). The three vertical lines mark the energies corresponding to the excitation wavelengths of 316 nm (3.92 eV; red line), 266 nm (4.66 eV; green line), and 216 nm (5.74 eV; blue line).

Focusing on the $v = 0$ spectra of Fig. 2, we have chosen three energy regions in order to illustrate the universality of our approach. These three regions are denoted by the three vertical lines displayed in the panels of Fig. 2. One energy region is centered at 266 nm (4.66 eV), where the $^3Q_0$ sub-band is clearly the dominant one. A second region is around 216 nm (5.74 eV), where the $^1Q_1$ sub-band dominates. Finally, we consider a third region around 316 nm (3.92 eV), at the tail of the spectra, where the yields of the I and I* channels are similar.

Optimization of the quantum yield of the I fragment channel at 266 nm

First, we maximize the yield of the I channel in the region around 266 nm, where the I* channel dominates. For this purpose, pulses of different duration, $\tau = 5$, 15, 30, and 60 fs, are applied to induce the photodissociation from the optimized initial wave functions formed as superpositions of the N lowest vibrational excitations of the CH_3–I stretching mode, where N

varies from 2 to 6. The vibrational quantum of energy of this mode is $E_1 - E_0 = 490.8\ \mathrm{cm}^{-1}$, where E_v is the energy of the v vibrational state. In the 266 nm energy region, CH_3I is mainly excited to the $^3Q_0$ state. After passing the conical intersection, the molecule dissociates producing mostly CH_3 + I* fragments. A much smaller amount of CH_3I + I products is formed (see the $v = 0$ panel of Fig. 2) as a result of the dissociation in $^1Q_1$ after a $^1Q_1 \leftarrow {}^3Q_0$ transition at the conical intersection, added to the fragmentation of the population initially excited to $^1Q_1$ and $^3Q_1$.

The results of maximizing the quantum yield of the I channel at 266 nm are shown in Fig. 3. The energy range of the four panels of Fig. 3 changes because it is related to the spectral bandwidth of the different pulses. For the 5 fs pulse, its spectral FWHM is 3536 cm^{-1}, while for the 60 fs pulse, the bandwidth is 295 cm^{-1}, twelve times smaller. The I channel cross sections $\sigma^{\mathrm{I}}_{\mathrm{op}} = \mathbf{c}^{\top}_{\mathrm{op}}\mathbf{S}^{\mathrm{I}}\mathbf{c}_{\mathrm{op}}$, displayed in the panels for three of the optimal initial superpositions, show the energy range covered by the superpositions. For the ground state $v = 0$, labelled as $N = 1$, the I channel quantum yield can be as small as 0.1. This result should be taken as the reference value in order to assess the degree of control achieved with the optimized initial superpositions. Interestingly, already with the $N = 2$ superposition (including $v = 0$ and 1), the I channel yield increases typically up to 0.7–0.9. And for $N \geq 3$ the yield becomes 1 or nearly 1 in practically all the relevant excitation energy range, which implies maximizing the I yield by a factor as large as 9–10 with respect to the $N = 1$ initial state. Therefore, by optimizing the initial superposition state, one can fully revert the fraction of fragments in the ground state I, over that in the excited state I*. Remarkably, throughout the spectral region encompassing the pump pulse bandwidth, one can obtain quantum yields very close to unity, using only the three lowest vibrational states, regardless of the pump pulse duration. This degree of control is probably only possible when the superposition state involves excitations of the CH_3–I stretching mode, which correlates with the reaction coordinate.

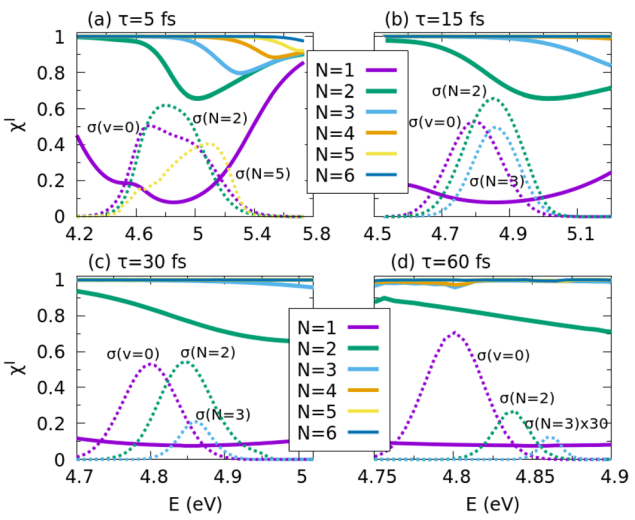

Fig. 3 Optimized quantum yields of the I fragment channel at 266 nm. Quantum yields of the I channel obtained when the CH_3I photodissociation process starts from optimized initial superpositions of N vibrational states in the CH_3–I stretching mode, which are excited at 266 nm by laser pulses of different duration (full width at half maximum) of (a) $\tau = 5$ fs, (b) $\tau = 15$ fs, (c) $\tau = 30$ fs, and (d) $\tau = 60$ fs. Each panel shows the results for six different optimal initial superpositions, including the $v = 0$ ($N = 1$), $v = 0$, 1 ($N = 2$), $v = 0$–2 ($N = 3$), $v = 0$–3 ($N = 4$), $v = 0$–4 ($N = 5$), and $v = 0$–5 ($N = 6$) vibrational states. The optimized photodissociation cross sections for channel I $\sigma^{\mathrm{I}}_{\mathrm{op}} = \mathbf{c}^{\top}_{\mathrm{op}}\mathbf{S}^{\mathrm{I}}\mathbf{c}_{\mathrm{op}}$, are also displayed in each panel for three initial superpositions, $N = 1$, 2, and 5 or $N = 1$, 2, and 3 (dashed lines). The $\sigma^{\mathrm{I}}_{\mathrm{op}}$ cross section obtained For $N = 3$ with the 60 fs pulse is multiplied by a factor of 30.

For the control to be possible, different pathways must connect the initial states with the same final scattering state at energy $E_{\mathrm{final}} = E_v + \hbar\omega_{\mathrm{blue}} = E_{v+1} + \hbar\omega_{\mathrm{red}}$, where ω_{blue} and ω_{red} are blue-shifted or red-shifted components of the pump pulse. Broadband pulses allow this interference between vibrational states to happen naturally. Indeed, the energy difference between $v = 0$ and $v = 5$ for the CH_3–I stretching mode is 2472 cm^{-1}, which can be covered by the bandwidth of the 5 and 15 fs pulses. Thus, pathways emerging from all these states can interfere between themselves and contribute almost equally. This is not the case for pulses of 60 fs (or even for 30 fs). The bandwidth of a 60 fs pulse allows interference only between energetically adjacent vibrational states. Moreover, at an energy $E = E_0 + \hbar\omega$, the amplitude of the field that allows excitation from E_1, $\varepsilon(\omega - \omega_{\mathrm{CH_3\text{–}I}})$, is only ~0.05% of the peak amplitude, $\varepsilon(\omega)$. Control over the quantum yield of a given channel is achieved by almost suppressing the photodissociation in the other channel from the different vibrational states. This is the reason why, in controlling the yield, the value of the cross section in the I channel is mostly conserved with respect to the cross section obtained from the single $v = 0$ initial state, while the cross section in the I* channel is almost suppressed when using the shorter pulses ($\tau = 5$ and 15 fs). For these pulses, the interference terms between the different vibrational states [see eqn (4)] are strong, allowing to suppress the I* yield while still conserving the intensity of $\sigma^{\mathrm{I}}_{\mathrm{op}}$ as N increases. The I yield is maximized without reducing its cross section. For longer pulses, and particularly for $\tau = 60$ fs, the smaller bandwidth leads to remarkably fewer and weaker interference terms in eqn (4), which are much smaller than the diagonal terms except at the edges of the spectra for the different vibrational states (shown in Fig. 2), where $\sigma_v(E)$ is small. Hence, control over the yield can only be achieved at the expense of reducing the cross section of the I channel as N increases. That is, fewer molecules are excited, but those excited produce almost exclusively I fragments.

Optimization of the quantum yield of the I* and I fragment channels at 316 and 216 nm

In Fig. 4 the performance of the control scheme is illustrated at the two edges of the CH_3I A band, in the regions around 316 and 216 nm, by applying a $\tau = 5$ fs pulse. For excitations around 316 nm, the yields of the I and I* channels are very low (see the $v = 0$ panel of Fig. 2). The $N = 1$ ($v = 0$) yield of Fig. 4a and c show that up to 3.9 eV the I yield is completely dominant over the I* yield, but for larger excitation energies the situation is gradually inverted. Thus, this energy region reflects a similar situation for

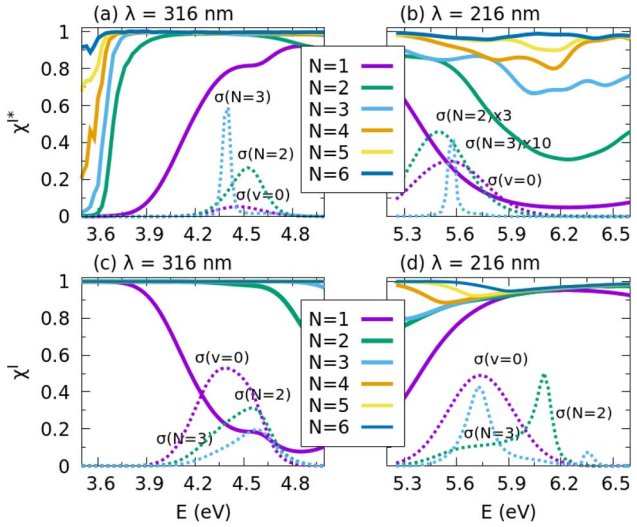

Fig. 4 Optimized quantum yields of the I* and I fragment channels at 316 and 216 nm. Quantum yields of the I* and I channels obtained when the CH_3I photodissociation process starts from optimized initial superpositions of N vibrational states in the CH_3–I stretching mode, which are excited at 316 nm (a) and (c) and at 216 nm (b) and (d) by a laser pulse with a duration (full width at half maximum) of $\tau = 5$ fs. Each panel shows the results for six different optimal initial superpositions, including the $v = 0$ ($N = 1$), $v = 0, 1$ ($N = 2$), $v = 0$–2 ($N = 3$), $v = 0$–3 ($N = 4$), $v = 0$–4 ($N = 5$), and $v = 0$–5 ($N = 6$) vibrational states. The optimized photodissociation cross sections for channel I* $\sigma^{I^*}_{op} = \mathbf{c}^{\top}_{op}\mathbf{S}^{I^*}\mathbf{c}_{op}$, and I $\sigma^{I}_{op} = \mathbf{c}^{\top}_{op}\mathbf{S}^{I}\mathbf{c}_{op}$, are also displayed in each panel for three initial superpositions, $N = 1$, 2, and 3 (dashed lines). The $\sigma^{I^*}_{op}$ cross section obtained for $N = 2$ and 3 in panel (b) are multiplied by a factor of 3 and 10, respectively.

the two channels in the absence of control, namely the passage of small yield to nearly unity or *vice versa*. When the control is exerted by optimizing the initial state, it is found that a yield of unity is achieved in practically all of the energy range for both fragmentation channels. Interestingly, a yield of unity is already obtained for most of the energies with the simplest and smallest $N = 2$ ($v = 0$ and 1) superposition. Moreover, in the case of the I* channel, the cross section $\sigma^{I^*}_{op}$ increases for $N = 2$ and 3 with respect to $N = 1$, as shown in Fig. 4a. Thus, the control scheme can maximize the yield of both channels in the same energy region, reverting situations of small (and nearly zero) yield to achieve yields of 1.

In the region around 216 nm, the I channel is dominant, as shown in the $v = 0$ panel of Fig. 2. This is reflected in the very high yield (typically >0.9) found for the single $v = 0$ initial state in the absence of control in Fig. 4d. The corresponding yield of the I* channel is typically <0.1, as shown in Fig. 4b. Clearly, no much more optimization of the I channel yield can be achieved by optimizing the initial superpositions, but still this yield is remarkably maximized at energies <5.7 eV when the size of the superposition is increased in Fig. 4d. The real maximization is achieved for the I* channel yield, which varies from typically less than 0.1 to nearly unity as N increases, as found in Fig. 4b. However, the maximization of the I* channel yield is obtained at the expense of reducing its absolute cross section, which decreases rapidly as N increases. The reason behind this result is similar to that governing the optimization with increasing N with a 60 fs pulse. The large difference between the cross sections of the I and I* channels at 216 nm (see the $v = 0$ panel of Fig. 2), with the I* cross section being very small, causes the terms of interference between the vibrational states to be small enough to prevent the suppression of the I yield, except at the edges of the spectra of the different v states, where the I* cross section also decreases remarkably. Using a pulse with a peak excitation energy around 5.3–5.4 eV (instead of the 5.74 eV associated with 216 nm), where the difference between the I and I* cross sections is not so large (as seen in the $v = 0$ spectra of Fig. 2), would lead to maximizing the I* yield up to unity without reducing significantly the I* cross section, resembling the situation found in Fig. 3a. We chose, however, the extreme situation for the I* channel at excitation energies around 216 nm in order to show that even in those unfavorable conditions our control scheme can maximize the yield of a channel with a very low intensity.

Experimental implementations

In the following, we discuss two possible experimental implementations. The scheme essentially consists of two steps: (a) preparation of the optimized initial superposition, and (b) excitation of the prepared superposition to the excited electronic states with a weak short visible-ultraviolet (VUV) laser pulse. Since the second step can be performed routinely nowadays,[18,20] we will focus on the first step.

The most direct method to prepare the superposition of vibrational states uses infrared (IR) lasers. In the case of the CH_3–I stretching mode, the carrier frequency must be near 500 cm^{-1}. Because the energy separation between the six lowest vibrational states is much larger than the pulse carrier frequency (~2500 cm^{-1} between $v = 0$ and $v = 5$), single-photon excitation of all the states by a broadband IR pulse is not possible. In addition, a weak field would not provide enough amplitude in the excited vibrational states to allow for an effective interference between them. Thus, a strong IR pulse will be needed to reach the upper states by multiphoton absorption. The duration of the pulse should be chosen to overcome the anharmonicity of the vibrational spectrum, which is just ~24 cm^{-1} in our case, for which a 19.6 μm picosecond pulse could be used. The optimization can be achieved by pulse shaping, applying an adaptive feedback genetic algorithm.[5,8,11,32] Indeed, the strategy is to generate the optimal combination of (complex) amplitudes in the different vibrational states of the initial superposition, such that these amplitudes interfere in the proper way to produce the desired final quantum yield. Such amplitudes can be prepared by using an IR pulse able to excite all the vibrational states of the superposition, properly shaped by the iterative adaptive feedback genetic algorithm to generate the required optimal combination. Although most acousto-optic modulators operate in the near IR,[62] some new techniques have been reported that can be used for pulses with wavelengths up to 20 μm as in our case.[63] Alternatively, free-electron laser facilities could be used to generate the required fields.[64,65]

This scheme can be substantially simplified when the initial superposition involves only two vibrational states, which can already improve the initial yield by more than 500% for most

energies, as shown in Fig. 3 and 4. Then the optimized superposition can be prepared by just controlling two parameters: the intensity of the IR pulse, that accounts for the relative populations in the superposition, and the time-delay between the IR pulse and the VUV pulse, which allows to fix the relative phase between the coefficients of the superposition at the time the wave packet is pumped to the excited state. No pulse shaper is then needed. The simplicity of this experimental scheme should endorse the possibility of its practical implementation.

Finally, a superposition of vibrational states can also be prepared by stimulated Raman using two ultrashort pulses.[29,66,67] In this case, the dynamics follows through a pump–dump–pump process, where the second pump can be identical to the first one. The first excursion in the excited dissociative states is used to displace the wave packet from the Franck–Condon region, creating the initial superposition, which can be further optimized using pulse shapers and genetic algorithms in the usual manner. The second excursion leads to fragmentation.

Conclusions

In summary, a robust control scheme to modify extensively the quantum yields of the different channels of a molecular nonadiabatic photodissociation process is proposed. The scheme relies on preparing and optimizing an initial coherent superposition of vibrational states of the molecule in the ground electronic state, which is pumped to the excited states by a simple weak ultrashort (fs), Gaussian-type laser pulse. Interference between the amplitudes of the optimized superposition is what allows maximization of the yields of the different fragmentation channels. The control scheme is applied to the CH_3I photodissociation in the A band, where it is shown that the scheme can maximize up to unity the yield of the two fragmentation channels of the process over the whole spectral range of the band. We show that the coherences encoded in the initial state are enough to guide the dynamics in this polyatomic molecule, under the presence of strong nonadiabatic (uncontrolled) couplings, such that absolute control over the quantum yield of any of the two fragmentation channels can be achieved. The control mechanism is based on destructive interference over the quantum pathways that lead to the undesired fragment. But using ultrashort pulses, we demonstrate that the high branching ratios are not achieved at the expense of small absolute photodissociation cross sections. Experimental implementations of the control scheme are suggested, some of them being simple enough as to guarantee its development in practice. The magnitude of the control effects found in this work is large enough as to be easily demonstrated experimentally. The proposed scheme is envisioned as general and universal in its application to molecular photodissociation processes.

Data availability

All the data related to this work are available upon request to the authors.

Author contributions

I. R. S. and A. G.-V. conceptualized and designed the project, performed the calculations, and wrote the manuscript.

Conflicts of interest

There are no conflicts to declare.

Acknowledgements

This research was supported by the Ministerio de Ciencia e Innovación of Spain (MICINN), Grant No. PID2021-122796NB-I00. This project has received funding from the COST Action CA21101 (COSY). The Centro de Supercomputación de Galicia (CESGA, Spain) is acknowledged for the use of its resources.

Notes and references

1 S. A. Rice and M. Zhao, *Optical Control of Molecular Dynamics*, Wiley, New York, 2000.
2 M. Shapiro and P. Brumer, *Quantum control of molecular processes*, John Wiley & Sons, Hoboken, 2012.
3 H. Rabitz, R. de Vivie-Riedle, M. Motzkus and K. Kompa, *Science*, 2000, **288**, 824–828.
4 T. Brixner and G. Gerber, *ChemPhysChem*, 2003, **4**, 418.
5 M. Wollenhaupt, V. Engel and T. Baumert, *Annu. Rev. Phys. Chem.*, 2005, **56**, 25–56.
6 G. G. Balint-Kurti, S. Zou and A. Brown, *Adv. Chem. Phys.*, 2008, **138**, 43–94.
7 V. Engel, C. Meier and D. J. Tannor, *Adv. Chem. Phys.*, 2009, 29–101.
8 C. Brif, R. Chakrabarti and H. Rabitz, *New J. Phys.*, 2010, **12**, 075008.
9 D. Townsend, B. J. Sussman and A. Stolow, *J. Phys. Chem. A*, 2011, **115**, 357–373.
10 P. v. d. Hoff, S. Thallmair, M. Kowalewski, R. Siemering and R. d. Vivie-Riedle, *Phys. Chem. Chem. Phys.*, 2012, **14**, 14460–14485.
11 I. R. Sola, B. Y. Chang, S. A. Malinovskaya and V. S. Malinovsky, *Adv. At., Mol., Opt. Phys.*, 2018, **67**, 151–256.
12 A. Gedanken and M. D. Rowe, *Chem. Phys. Lett.*, 1975, **34**, 39–43.
13 D. W. Chandler and P. L. Houston, *J. Chem. Phys.*, 1987, **87**, 1445–1447.
14 A. T. J. B. Eppink and D. H. Parker, *J. Chem. Phys.*, 1998, **109**, 4758–4767.
15 A. T. J. B. Eppink and D. H. Parker, *J. Chem. Phys.*, 1999, **110**, 832–844.
16 M. H. M. Janssen, M. Dantus, H. Guo and A. H. Zewail, *Chem. Phys. Lett.*, 1993, **214**, 281–289.
17 P. C. Samartzis, B. L. G. Bakker, D. H. Parker and T. N. Kitsopoulos, *J. Phys. Chem. A*, 1999, **103**, 6106–6113.
18 R. de Nalda, J. Durá, A. García-Vela, J. G. Izquierdo, J. González-Vázquez and L. Bañares, *J. Chem. Phys.*, 2008, **128**, 244309.

19 L. Rubio-Lago, A. García-Vela, A. Arregui, G. A. Amaral and L. Bañares, *J. Chem. Phys.*, 2009, **131**, 174309.
20 A. García-Vela, R. de Nalda, J. González-Vázquez and L. Bañares, *J. Chem. Phys.*, 2011, **135**, 154306.
21 C. Hu, S. Pei, Y.-L. Chen and K. Liu, *J. Phys. Chem. A*, 2007, **111**, 6813–6821.
22 M. Shapiro and R. Bersohn, *J. Chem. Phys.*, 1980, **73**, 3810–3817.
23 H. Guo, *J. Chem. Phys.*, 1992, **96**, 6629–6642.
24 A. D. Hammerich, U. Manthe and R. Kosloff, *J. Chem. Phys.*, 1994, **101**, 5623–5646.
25 C. R. Evenhuis and U. Manthe, *J. Phys. Chem. A*, 2011, **115**, 5992–6001.
26 Y. Amatatsu, K. Morokuma and S. Yabushita, *J. Chem. Phys.*, 1991, **94**, 4858–4876.
27 Y. Amatatsu, S. Yabushita and K. Morokuma, *J. Chem. Phys.*, 1996, **104**, 9783–9794.
28 D. Xie, H. Guo, Y. Amatatsu and R. Kosloff, *J. Phys. Chem. A*, 2000, **104**, 1009.
29 D. J. Tannor and S. A. Rice, *J. Chem. Phys.*, 1985, **83**, 5013–5018.
30 D. Tannor, R. Kosloff and S. A. Rice, *J. Chem. Phys.*, 1986, **85**, 5805.
31 P. Brumer and M. Shapiro, *Chem. Phys. Lett.*, 1986, **126**, 541–546.
32 R. S. Judson and H. Rabitz, *Phys. Rev. Lett.*, 1992, **68**, 1500.
33 A. Assion, T. Baumert, M. Bergt, T. Brixner, B. Kiefer, V. Seyfried, M. Strehle and G. Gerber, *Science*, 1998, **282**, 919.
34 P. Anfirud, R. de Vivie-Riedle and V. Engel, *Proc. Natl. Acad. Sci. U. S. A.*, 1999, **96**, 8328–8329.
35 T. Brixner, N. H. Damrauer, P. Niklaus and G. Gerber, *Nature*, 2001, **414**, 57.
36 R. J. Levis, G. M. Menkir and H. Rabitz, *Science*, 2001, **292**, 709.
37 C. Daniel, J. Full, L. González, C. Lupulescu, J. Manz, A. Merli, S. Vajda and L. Wöste, *Science*, 2003, **299**, 536–539.
38 M. Sukharev and T. Seideman, *Phys. Rev. Lett.*, 2004, **93**, 093004.
39 B. J. Sussman, D. Townsend, M. Y. Ivanov and A. Stolow, *Science*, 2006, **314**, 278–281.
40 H. Goto, H. Katsuki, H. Ibraim, H. Chiba and K. Ohmori, *Nat. Phys.*, 2011, **7**, 383–385.
41 L. S. Cederbaum, Y.-C. Chiang, P. V. Demekhin and N. Moiseyev, *Phys. Rev. Lett.*, 2011, **106**, 123001.
42 A. García-Vela, *J. Phys. Chem. Lett.*, 2012, **3**, 1941–1945.
43 M. E. Corrales, J. González-Vázquez, G. Balerdi, I. R. Sola, R. de Nalda and L. Bañares, *Nat. Chem.*, 2014, **6**, 785.
44 A. García-Vela and N. E. Henriksen, *J. Phys. Chem. Lett.*, 2015, **6**, 824–829.
45 M. E. Corrales, R. de Nalda and L. Bañares, *Nat. Commun.*, 2017, **8**, 1345.
46 A. García-Vela, *Phys. Rev. Lett.*, 2018, **121**, 153204.
47 A. Serrano-Jiménez, L. Bañares and A. García-Vela, *Phys. Chem. Chem. Phys.*, 2019, **21**, 7885.
48 K. B. Møller, N. E. Henriksen and A. H. Zewail, *J. Chem. Phys.*, 2000, **113**, 10477–10485.
49 B. Amstrup and N. E. Henriksen, *J. Chem. Phys.*, 1992, **97**, 8285–8295.
50 S. Meyer and V. Engel, *J. Phys. Chem. A*, 1997, **101**, 7749–7753.
51 N. Elghobashi and L. González, *Phys. Chem. Chem. Phys.*, 2004, **6**, 4071–4073.
52 B. Y. Chang, S. Shin and I. R. Sola, *J. Phys. Chem. Lett.*, 2015, **6**, 1724–1728.
53 B. Y. Chang, S. Shin and I. R. Sola, *J. Chem. Theory Comput.*, 2015, **11**, 4005–4010.
54 B. Y. Chang, S. Shin and I. R. Sola, *J. Phys. Chem. A*, 2015, **119**, 9091–9097.
55 B. Y. Chang, S. Shin, V. Engel and I. R. Sola, *J. Phys. Chem. A*, 2017, **121**, 8280–8287.
56 C. G. Arcos, A. García-Vela and I. R. Sola, *J. Phys. Chem. Lett.*, 2024, **15**, 1442.
57 A. B. Alekseyev, H.-P. Liebermann, R. J. Buenker and S. N. Yurchenko, *J. Chem. Phys.*, 2007, **126**, 234102.
58 A. B. Alekseyev, H.-P. Liebermann and R. J. Buenker, *J. Chem. Phys.*, 2007, **126**, 234103.
59 G. G. Balint-Kurti, R. N. Dixon and C. C. Marston, *J. Chem. Soc., Faraday Trans.*, 1990, **86**, 1741.
60 G. G. Balint-Kurti, R. N. Dixon and C. C. Marston, *Int. Rev. Phys. Chem.*, 1992, **11**, 317.
61 R. Schinke, *Photodissociation Dynamics: Spectroscopy and Fragmentation of Small Polyatomic Molecules*, Cambridge University Press, Cambridge, 1993.
62 A. M. Weiner, *Rev. Sci. Instrum.*, 2000, **71**, 1929–1960.
63 A. Cartella, S. Bonora, M. Först, G. Cerullo, A. Cavalleri and C. Manzoni, *Opt. Lett.*, 2014, **39**, 1485–1488.
64 P. O'Shea and H. Freund, *Science*, 2001, **292**, 1853–1858.
65 C. Feng and H.-X. Deng, *Nucl. Sci. Tech.*, 2018, **29**, 160.
66 L. Dhar, J. A. Rogers and K. A. Nelson, *Chem. Rev.*, 1994, **94**, 157–193.
67 U. Banin, A. Bartana, S. Ruhman and R. Kosloff, *J. Chem. Phys.*, 1994, **101**, 8461–8481.